# Influence of nonlinearities on the power output of the Self-Oscillating Fluidic Heat Engine (SOFHE)

**A Tessier-Poirier[1,2] , T Monin[1,2,3,4], E Léveillé[1,2] F Formosa[3], S Monfray[4], and L G Fréchette[1,2]**

E-mail: Luc.Frechette@usherbrooke.ca
[1] 3IT, Université de Sherbrooke, Sherbrooke, QC, Canada
[2] LN2, CNRS UMI-3463, Université de Sherbrooke, Canada
[3] SYMME, Université Savoie Mont-Blanc, Annecy-le-Vieux, France
[4] STMicroelectronics, Crolles, France

**Abstract.** In this paper, it is shown that two non-linearities drive the oscillations amplitude and the potential power density of the Self-Oscillating Fluidic Heat Engine (SOFHE). This new type of engine converts thermal energy into mechanical energy by producing self-sustained oscillations of a liquid column from a continuous heat source to power wireless sensors from waste heat. The underlying theoretical modeling shows that the pressure and the temperature nonlinearities limit the final oscillations amplitude, hence its achievable power density.

## 1. Introduction

The new paradigm of the Internet of things (IoT) leads to a multiplication of sensors everywhere in our environment. Powering those wireless sensors longer than a battery life can be done by harvesting nearby energy sources. In this paper, a new type of thermal energy harvester inspired by [1] is studied, the Self-Oscillating Fluidic Heat Engine (SOFHE) [2, 3], which couples an electro-mechanical transducer to a motor based on the self-oscillatory phenomenon observed in the pulsating heat pipes (PHP) [4]. The motor in SOFHE consists of a small tube closed at one end, filled with water (figure 1). By heating the closed-end, evaporation of the liquid leads to the formation of a vapor bubble which increases in length until an equilibrium position is reached. From this equilibrium, increasing the temperature of the heat source leads to an instability [5], the liquid column starts to oscillate as shown by the experimental pressure measurements in figure 2 from [2]. This paper shows that the final amplitude of the oscillations and the power output of the SOFHE are limited by the gas pressure and the wall temperature nonlinearities.

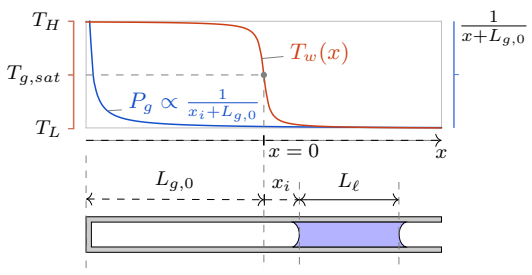


Figure 1: Tube, pressure and temperature.

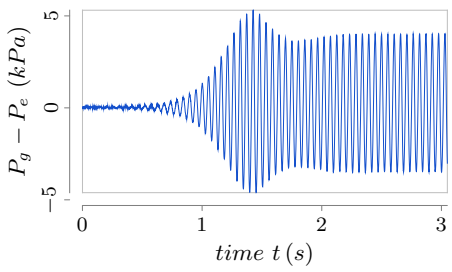


Figure 2: Start-up of the oscillations.

## 2. Model of the self-oscillations

Newton's second law is applied to the liquid column Eq. (1), where movement of the column ($x_i$) will result from the difference between the gas bubble pressure ($P_g$) in Eq. (2) and the external pressure $P_e$ and be opposed by the liquid's friction ($F_f$) assuming Poiseuille flow (Eq. (3)) and the harvester, taken as a linear damping ($F_h = c_h \dot{x}_i$ where $c_h \leqslant 0$). In Eq. (2), the mass of vapor $m_g$ change accordingly to the evaporation/condensation rate which is modelled from the heat conduction (with a thermal resistance $R_{th}$ and the enthalpy of vaporization $H_v$) to the meniscus location, leading to the first part of Eq. (6). The value of the thermal resistance $R_{th}$ should come from experiment or theoretical estimation. The wall temperature $T_w$ is constant in the heat source at $T_H$ and at the heat sink at $T_L$ and varies linearly between those two regions. This is modelled by an arctangent as shown in figure 1 and given by Eqs. (4) and (5).

$$\ddot{x}_i = (1/m_\ell)\,(P_g\,A - P_e\,A + F_f + F_h) \quad (1) \qquad F_f = -\,8\pi\,\mu\,L_\ell\,\dot{x}_i = \;c_f\,\dot{x}_i \quad (3)$$

$$P_g = m_g\,R_g\,T_g/\left((x_i + L_{g,0})\;A\right) \quad (2) \qquad T_w = A_{th}\,\arctan(M_{th}\cdot x + B_{th}) + C_{th} \quad (4)$$

$$A_{th} \equiv (T_H - T_L)/\pi \quad (5a) \qquad M_{th} \equiv 1/A_{th}\,\left(B_{th}^2 + 1\right)\cdot (dT/dx)_{x=0} \quad (5c)$$

$$C_{th} \equiv (T_H + T_L)/2 \quad (5b) \qquad B_{th} \equiv \tan\left[(T_{g,sat,0} - C_{th})/A_{th}\right] \quad (5d)$$

$$\dot{m}_g = \frac{\dot{Q}}{H_v} = \frac{T_{wall}(x_i) - T_{g,sat}}{H_v R_{th}} = \frac{A_{th}}{H_v R_{th}}\,\arctan(M_{th}\cdot x_i + B_{th}) + \frac{C_{th} - T_{g,sat}}{H_v R_{th}} \quad (6)$$

The equilibrium solution of these equations is a constant $x_i$ such that $T_{wall}(x_i) = T_{g,sat}$, leading to $x_i = \dot{x}_i = \dot{m}_g = 0$. It is useful to study variations of the system relative to this equilibrium and to nondimensionalized the problem with $L_{g,0}$ and the natural angular frequency $\omega_n$ (7f), leading to Eq. (8a) (nonlinear because of $P_g$) and Eq. (8c) (nonlinear because of the arctan $T_w$ profile). It is useful to study the effect of the nonlinearities. In that purpose, we can compare the nonlinear equations (8a) and (8c) to their linearized counterpart given by Eqs. (8b) and (8d). Finally, the harvester extracts an adimensionalized power $\widetilde{\mathcal{P}_h}$ given by Eq. (9).

$$\widetilde{x_i} \equiv x_i/L_{g,0} \quad (7a) \qquad \dot{\widetilde{x}}_i \equiv (1/(\omega_n L_{g,0}))\,\dot{x}_i \quad (7e) \qquad \widetilde{\Delta m_g} \equiv (m_g - m_{g,0})/m_{g,0} \quad (7i)$$

$$\tau \equiv \omega_n\,t \quad (7b) \qquad \omega_n \equiv (P_{g,0}/\rho_\ell\,L_\ell\,L_{g,0})^{1/2} \quad (7f) \qquad \widetilde{\omega} \equiv \omega/\omega_n \quad (7j)$$

$$\widetilde{M_{th}} \equiv L_{g,0}M_{th} \quad (7c) \qquad \widetilde{C_{th}} \equiv (C_{th} - T_{g,sat})/T_C \quad (7g) \qquad \zeta_f \equiv -c_f/(2\omega_n m_\ell) \quad (7k)$$

$$\widetilde{A_{th}} \equiv A_{th}/T_C \quad (7d) \qquad \zeta_h \equiv -c_h/(2\omega_n m_\ell) \quad (7h) \qquad T_C \equiv \omega_n\,m_{g,0}\,H_v\,R_{th} \quad (7l)$$

$$\ddot{\widetilde{x}}_i = -\left(\frac{1}{1+\widetilde{x}_i}\right)\widetilde{x}_i + \left(\frac{1}{1+\widetilde{x}_i}\right)\widetilde{\Delta m_g} - 2\,(\zeta_f + \zeta_h)\;\dot{\widetilde{x}}_i \quad (8a)$$

$$\ddot{\widetilde{x}}_i = -\widetilde{x}_i + \widetilde{\Delta m_g} - 2\,(\zeta_f + \zeta_h)\;\dot{\widetilde{x}}_i \quad (8b)$$

$$\dot{\widetilde{\Delta m_g}} = \widetilde{A_{th}}\,\arctan(\widetilde{M_{th}}\cdot\widetilde{x}_i + B_{th}) + \widetilde{C_{th}} \quad (8c)$$

$$\dot{\widetilde{\Delta m_g}} = \left(\widetilde{A_{th}}\widetilde{M_{th}}/(1 + {B_{th}}^2)\right)\;\widetilde{x}_i \quad (8d)$$

$$\widetilde{\mathcal{P}_h} \equiv \left(\pi/{\omega_n}^3 m_\ell\,{L_{g,0}}^2\right)\;\mathcal{P}_h = \widetilde{\omega}\,\zeta_h\int_\tau^{\tau+2\pi/\widetilde{\omega}} {\dot{\widetilde{x}}_i}^2\,d\tau \quad \approx \pi\,\zeta_h\,{\dot{\widetilde{X}}_i}^2 = \pi\,\widetilde{\omega}^2\,\zeta_h\,{\widetilde{X}_i}^2 \quad (9)$$

## 3. The amplitude of the limit cycle is driven by the nonlinearities

As expected, numerical simulations of the linear equations (8b) and (8d) show an exponential growth with no saturation. Including either one or the other nonlinearity does lead to saturation of the amplitude. In the saturated regime, the variables $\widetilde{x_i}$, $\dot{\widetilde{x}}_i$ and $\dot{\widetilde{\Delta m}}_g$ varie nearly periodically and is assumed to be reached when their difference between two consecutive cycle is less then 0.1% on all the cycle for ten consecutive cycles. The saturated regime is shown by the orbits from numerical simulations in figure 3 for two cases (see table 1).

Table 1: Numerical value of the parameters for two studied cases

| | $\zeta_f$ | $\widetilde{A_{th}}$ | $\widetilde{M_{th}}$ | $B_{th}$ | $\widetilde{C_{th}}$ | Conclusions |
|---|---|---|---|---|---|---|
| Case 1 | 0.0217 | 0.0043 | -14.50 | 0.3792 | -0.0016 | $T_N$ dominates over $P_N$ |
| Case 2 | 0.0034 | 0.0271 | -0.3625 | 0.3792 | -0.0098 | $P_N$ dominates over $T_N$ |

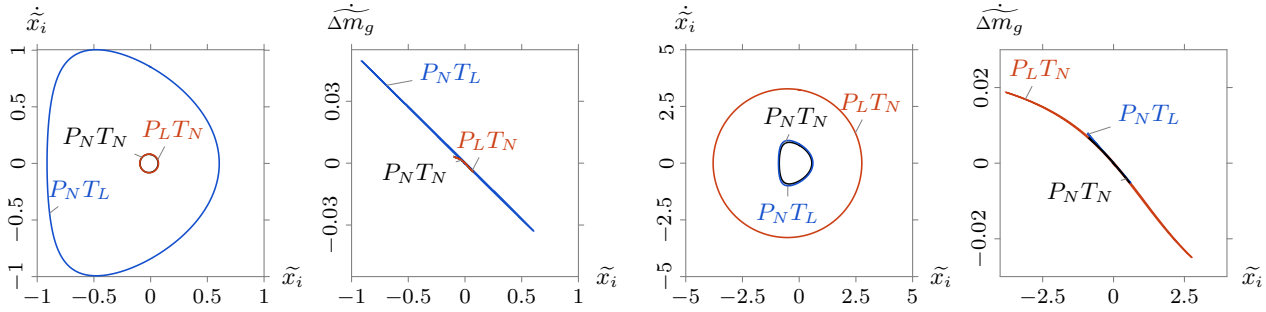


(a) case 1 (b) case 1 (c) case 2 (d) case 2

Figure 3: Saturated regime for $\zeta_h = 0$ with parameters of table 1.

### *3.1. Wall Temperature Profile nonlinearity*

As the meniscus oscillates at small amplitude, the wall temperature profile seen by the meniscus is mostly linear (figure 1). As the amplitude increase, however, the wall temperature increase/decrease less than linearly ($T_w$ saturates, (4)). This leads to a saturation of the evaporation/condensation (8c) and therefore, of the injection of energy into the system. Since the dissipation of energy is linear, the system eventually reach an amplitude where the injection of energy and the dissipation of energy equals each other over a cycle. The behavior of this saturated regime (with only the $T_w$ nonlinearity is shown in figure 3 by the curves denoted $P_LT_N$. A saturation of $\dot{\widetilde{\Delta m}}_g$ should be seen by plotting it against $\widetilde{x_i}$, given Eq. (8c). This signature is indeed observed as shown by the curve $P_LT_N$ in figure 3d. Such behavior in experimental measurements could indicate the dominance of the $T_w$ nonlinearity.

### *3.2. Pressure nonlinearity*

When the meniscus oscillates, the compression/expansion of the gas gives rise to variations of the pressure $P_g$ with $\Delta P_g \propto 1/(x_i + L_{g,0})$ (as shown in Eqs. (2), (8a) and in the figure 1). For oscillations of small amplitude at constant mass, $P_g$ is proportional to the volume variation : $P_g \propto x_i$. As the amplitude increases, however, this linear approximation is not valid anymore. As the meniscus goes toward the closed end ($x_i \to -L_{g,0}$), the pressure tends to infinity (as shown in figure 1), preventing the liquid column to go touch the closed end. This nonlinear behavior limits the evaporation/condensation rate and forces the system to settle on a saturated regime as shown by the $P_NT_L$ curve on figure 3a. The saturated regime exhibit an asymmetry along $\widetilde{x_i}$ on the plane $(\widetilde{x_i}, \dot{\widetilde{x}}_i)$, a signature due to the presence of the closed end. As it reaches the closed end, the system bounces back, reverses its velocity on a short distance.

*3.3. Pressure and Wall Temperature nonlinearities combined - Amplitude and Power*
The combination of both nonlinearities leads to a saturated regime shown by the $P_NT_N$ curves in figure 3. In case 1, figures 3a and 3b, suppressing the pressure nonlinearity (the $P_LT_N$ curve which only contains the temperature nonlinearity) has so little effect on the size of the saturated regime that the two curves $P_NT_N$ and $P_LT_N$ are almost undistinguishable. However, suppressing the temperature nonlinearity (the $P_NT_L$ curve) changes drastically the amplitude of the saturated regime. One concludes that the wall temperature nonlinearity is dominant. Incidentally, the $P_NT_N$ curve is exhibiting a wall temperature nonlinearity signature and no pressure nonlinearity signature. Now, from case 1, taking a $\zeta_h > 0$ allows to produce a power $\widetilde{\mathcal{P}_h}$ given by (9). By assuming a sinusoidal motion, we get the approximation in (9) which clearly shows that for a given $\zeta_h$ and a given $\widetilde{\omega}$, the power $\widetilde{\mathcal{P}_h}$ will increase if the size of the saturated regime increases (the peak amplitude of $\widetilde{x_i}$ and $\dot{\widetilde{x}}_i$, $\widetilde{X_i}$ and $\dot{\widetilde{X}}_i$ respectively, increase). The optimal $\zeta_h$ (which produce the maximal power) leads to $\widetilde{\mathcal{P}_h}(P_NT_N) = 23$, $\widetilde{\mathcal{P}_h}(P_LT_N) = 24$ and $\widetilde{\mathcal{P}_h}(P_NT_L) = 5250$. Just like for the amplitude, suppressing either nonlinearity increases the power but the temperature nonlinearity is clearly dominant.

Going from case 1 to case 2 is the adimensionnal equivalent of dividing $L_{g,0}$ by 40 and keeping all the other dimensional parameters of the equations constants. The equilibrium is therefore closer to the closed end and the pressure nonlinearity becomes more apparent. This is shown in figures 3c and 3d where the pressure nonlinearity is now clearly dominant (suppressing the temperature nonlinearity as much less influence on the size of the saturated regime). This could have been concluded from the $P_NT_N$ curve shape in figure 3c, which exhibit a nonlinear pressure signature. In case 2, the optimal $\zeta_h$ leads to $\widetilde{\mathcal{P}_h}(P_NT_N) = 631$, $\widetilde{\mathcal{P}_h}(P_LT_N) = 5750$ and $\widetilde{\mathcal{P}_h}(P_NT_L) = 848$. Again, just like for the amplitude, suppressing either nonlinearity increase the power but the pressure nonlinearity is now clearly dominant. One may conclude that one non-linearity can dominate over the other to set the amplitude and the power output, depending on the parameters of the system.

## 4. Conclusion
A nondimensional model of the SOFHE was presented which include two nonlinearities and a linear harvester. It has been shown that the final amplitude of the system without harvesting is limited by the nonlinearities. Furthermore, one nonlinearity can dominate over the other (have more impact on the final amplitude than the other). Finally, it has been shown that the nonlinearities also limits the power output. In this paper, the focus was solely on the nonlinearity but the power output also depends on the linear part. It will eventually be useful to show and understand the influence of the adimensional numbers on the amplitude and on the power output, leading to design guidelines for the SOFHE.

## Acknowledgments
This research was funded by NSERC and conducted in collaboration with STMicroelectronics. We are grateful to Thomas Skotnicki from STMicroelectronics for discussions on the subject.

## References
[1] Léveillé *et al.* 2012 *PowerMEMS 2012* (Atlanta)
[2] Monin T *et al.* 2016 *PowerMEMS 2016* (Paris)
[3] Skotnicki T 2013 Thermoelectric generator
[4] Das S P *et al.* 2010 *Int. J. Heat Mass Transfer* **53** 3905–3913
[5] Jenkins A J 2013 *Physics Reports* **525** 205–207